Bridging in co-cured composite joints

Charline van Innis[1*], Michal K. Budzik[2], Thomas Pardoen[1,3]

[1]*Institute of Mechanics, Materials and Civil Engineering (iMMC), UCLouvain, Louvain-la-Neuve, Belgium (charline.vaninnis@uclouvain.be , thomas.pardoen@uclouvain.be)*

[2]*Department of Mechanical and Production Engineering (MPE), Aarhus University, Aarhus, Denmark (mibu@mpe.au.dk)*

[3]*Wel Research Institute, avenue Pasteur, 6, 1300 Wavre, Belgique*

**Corresponding author: charline.vaninnis@uclouvain.be*

ABSTRACT

Further deployment of advanced polymer-based composites in critical structures requires, among others, new progress in adhesive bonding solutions from processing to performance. Among others, the cost and time intensity of manufacturing can be mitigated through co-curing of composite elements using a thermoplastic film, typically a Polyetherimide (PEI) film. However, the use of PEI films in resin transfer moulding leads to low toughness (<500 J/m²). The objective of this work is to improve the toughness of co-cured composite joints by inserting UHMPE filaments between a PEI film and the composite panels in order to trigger crack bridging and a significant R-effect. The influence of the spacing and of the tensile strength of the filaments has been determined experimentally, resulting in an increase of the toughness by up to a factor 3. In addition, the influence of these parameters has been further investigated with a closed-form crack propagation model. Decreasing the spacing and increasing the strength of the filaments enhances the joint toughness. Increasing the tensile elongation of the filaments results in a less steep R-effect, requiring a longer crack propagation to attain of the maximum fracture toughness.

Keywords: co-curing, composite joints, toughening, bridging

1. Introduction

Carbon fibre reinforced polymer composites (CFRPs) are widely used in advanced structural composites such as in airplanes, wind turbine blades or marine structures, owing to high strength and stiffness to weight ratios. Manufacturing these structures often requires the joining of CFRP-based elements. Mechanical fastening is one option but drilling holes in the adherents lowers the structural integrity due to stress concentrations (Pocius, 2012). Adhesive bonding offers more homogeneous stress transfer and lightweight. However, adhesives often suffer from limited mode I toughness G_{Ic} as well as cost and time intensive bonding process (Pocius, 2012), preventing a generalized use of this joining technique.

Co-curing is an alternative to secondary adhesive bonding, involving lower manufacturing intensity. Co-curing consists in the simultaneous curing and bonding of the composite parts. In secondary bonding, the adherents are first cured apart, and the surfaces are treated before the CFRPs adherents can be bonded together. Co-curing is only possible when no resin has to be injected during the process otherwise the adhesive would flow out of the bondline region. Hence, co-curing is possible using pre-pregs, but not with a resin transfer moulding process (RTM). Co-cured composite joints are known to be characterized by a lower mode I fracture toughness compared to secondary bonded joints due to the generation of defects at the adhesive/composite interface (Anders et al., 2019, 2017; Kermani et al., 2020). Now, on the opposite side, co-curing results in better geometrical accuracy (Kim et al., 2010) of the components and are less affected by hygrothermal ageing (Brito et al., 2020).

In order to improve the G_{Ic} of co-cured composite joints, Quan and co-workers (Quan et al., 2023, 2022) suggested replacing the adhesive by a thermoplastic film compatible with the composite resin (Deng et al., 2015). This led Quan and co-workers to insert polyetherimide (PEI) and UV-treated polyetheretherketone (PEEK) films between pre-pregs made of the 8552 epoxy resin. Regarding PEI co-cured joints, at room temperature, an enhanced mode I toughness was reported compared to the composite toughness during delamination, but lower than the G_{Ic} of the co-cured adhesive joint. However, the PEI film results in higher mode II fracture toughness (G_{IIc}) and lap-shear strength compared to composite delamination with an adhesive-based co-cured joint. In addition, increasing the PEI film thickness improves both the mode I and mode II fracture toughness as well as the lap-shear strength with an optimum thickness around 200 µm. The good adherence between the composites and the PEI results from the interdiffusion of PEI and epoxy during curing. Other candidates for co-curing include, among others, phenoxy (Van Velthem et al., 2015), polyethersulfone (PES) (Cheng et al., 2019; Van Velthem et al., 2015) and polysulfone (PSU) (Min and Kim, 1999). Recently, we co-cured composite joints using PEI films of varying thicknesses (as reported in Supplementary Material 1). However, these co-cured joints also suffer from low mode I fracture toughness when compared to the composite delamination toughness, requiring the exploration of effective toughening strategies.

Several toughening strategies have been investigated in the literature for adhesive joints. The first consists in enhancing the plastic energy dissipation in the joint by increasing the adhesive thickness (Bascom et al., 1975; Kinloch and Shaw, 1981; Martiny et al., 2012; Pardoen et al., 2005). Plastic energy dissipation can also be favoured by inserting a softer layer close to the crack propagation plane in the assembly (Dépinoy et al., 2019). Crack deflection by architecturing the adherents has been proven effective to raise the mode I fracture toughness through forcing local mode-mixity at the crack tip (Cordisco et al., 2016; Maloney and Fleck, 2018; Reedy, 2008; Zavattieri et al., 2007). A crack can also be deflected from the propagation plane by adding stiff particles or cavities. If a cavity is added, it can trap the crack and if large enough, it blunts the crack, delaying its reinitiation and increasing the effective G_{Ic} (Heide-Jørgensen and Budzik, 2018; Maloney and Fleck, 2019). It has even been suggested to create arrays of cavities referred as pillar interfaces (Heide-Jørgensen et al., 2020). Following this idea, more generally, the bondline can be structured using metamaterials concepts (Athanasiadis et al., 2021; Hedvard et al., 2024) to trigger complex failure modes. Elastic heterogeneities (Kendall, 1975; Xia et al., 2013) are also known to influence the effective G_{Ic} and can be achieved by architecturing the adherents (Morano et al., 2020). Finally, a mechanism that has proven very efficient is crack bridging.

Bridging takes place in composites owing to fibres attached to both crack faces behind the crack tip. It can also be triggered by adding Z-pins (Cartié et al., 2006; Hoffmann and Scharr, 2018), by inserting a carrier in the adhesive (Heide-Jørgensen et al., 2018; Maloney and Fleck, 2019; Yudhanto et al., 2020) or by changing the local adherence at both interfaces (Maloney and Fleck, 2019; Tao et al., 2022). In composite parts, thermoplastic veils[1] (Kuwata and Hogg, 2011; Quan et al., 2020) are also often introduced at interplies to trigger bridging and to improve the delamination toughness. The areal weight of such veils is known to have an influence on G_{Ic} with an existing optimum areal weight above which G_{Ic} decreases. The resulting toughness varies depending on the thermoplastic from which the veil is made and on the architecture of the carbon fibre fabrics (e.g. unidirectional UD, H5-satin or non-crimp fibre NCF). For example, Quan et al. (Quan et al., 2020) reported a larger toughening effect of UD composites compared to NCF and H5-satin laminates. Bridging is the toughening principle addressed in the present study.

Several models have been developed to predict the mechanical response of structures involving fibre bridging (Accornero et al., 2022; Carpinteri, 1984; Cox and Marshall, 1994, 1991; Li et al., 2021; Sørensen and Jacobsen, 1998; Spearing and Evans, 1992). In the context of finite element analysis, cohesive zone models are often used with multilinear traction-separation laws (Khan, 2019). Analytical or closed-form models have also been proposed such

[1] Thermoplastic veils are films made of thermoplastic fibres, often non-woven fibres and are generally used to toughen composites in the interlaminar region.

as the one developed by Cox and Marshall (Cox and Marshall, 1994, 1991) or by Sørensen and Jacobsen (Sørensen and Jacobsen, 1998) who considered the continuous effect of bridging and non-discrete bridging events opposite to Spearing and Evans (Spearing and Evans, 1992), Szekrényes and Uj (Szekrényes and Uj, 2005) and Li et al. (Li et al., 2021). In these models, a bridging law relating the bridging stress to the opening displacement is required. The bridging law shape depends on the nature of the bridging mechanism and on the material of the bridging filaments. For instance, if pull-out takes place, the magnitude of the bridging stresses decreases with increasing opening displacement. One of the main issues in modelling bridging is the occurrence of snap-back instability upon failure of a filament resulting in a sudden decrease of the applied displacement and of the force as the energy released by the advancing crack exceeds the energy dissipated to form the new fracture surfaces (Li et al., 2021). Sequence linear analysis (Invernizzi et al., 2011) and crack length control schemes (Carpinteri and Accornero, 2018) are more adequate than a classical Newton-Raphson scheme to solve this category of mathematical problem.

The present work aims at toughening co-cured PEI composite joints. PEI is selected for co-curing because interdiffusion is observed in PEI-epoxy systems as reported in Supplementary Material 1 and by Voleppe et al. (Voleppe et al., 2021) and Farooq et al. (Farooq et al., 2023, 2021, 2020). Toughening is induced by triggering crack bridging by inserting polyethylene filaments perpendicular to the crack propagation direction. The influence of the bridging filament strength and spacing is investigated experimentally and modelled analytically using a discrete model considering each bridging event individually. Increasing the spacing between the filaments[2] and the tensile strength of the filaments results in a significant improvement of the fracture toughness. The tensile elongation of the bridging filaments has not been tested

[2] The words « cords » and « threads » are also used in what follows as synonym of filament. The so called filaments are made of elementary wires braided together.

experimentally but addressed based on the analytical model. Guidelines are given for the optimization of joints toughened through the addition of bridging filaments.

2. Materials and methods

2.1.Materials

The composite adherents are made of the Hexflow RTM6 epoxy resin (Hexcel, 2018) and HexForce G0926 H5-satin carbon fibres fabrics. The two composite adherents are co-cured and assembled in a RTM press. Between the two composite parts, a thermoplastic film with thermoplastic filaments are inserted (se Section 2.2). The thermoplastic film consists of 50 µm thick PEI film (Ultem 1000, Sabic, sold by GoodFellow, see Supplementary Material 1 for the choice of the thickness) and is degreased using acetone prior to co-curing. The filaments are made of ultra-high-molecular-weight polyethylene (UHMPE) from the brand *Caperlan* from Decathlon store are inserted between the carbon fabrics and the PEI film. These fishing lines are filaments made of several elemental strands braided together. Different diameters and ultimate tensile force (UTF) of filaments were tested, listed in Table 1. The adherence of these filaments to either RTM6 or PEI has not been characterized but a weak adhesion with PEI is expected while a good adhesion with RTM6 is anticipated owing the infiltration of the filaments by the resin. This will be discussed further when looking at the results in Section 3.

Table 1: Properties of the UHMPE filaments under the form fishing lines used to investigate the effect of filament UTF and spacing.

Fishing line	Description	Ultimate tensile force [N]	Diameter of the line (diameter of one filament) [mm]	Investigated spacing [mm]
Caperlan TX4 60µm	4 filaments braid	38 N (3.9 kg[3])	0.25 (0.06)	1, 2, 5, 7, 10
Caperlan TX8 60µm	8 filaments braid	56 N (5.7 kg)	0.19 (0.06)	1, 2
Caperlan TX8 100µm	8 filaments braid	81 N (8.3 kg)	0.25 (0.1)	1, 2
Caperlan TX8 200µm	8 filaments braid	167 N (17.2 kg)	0.35 (0.2)	1, 2

2.2. *Joints manufacturing*

Prior to joint manufacturing, the UHMPE filaments are manually positioned with fixed spacing on both sides of the PEI film. Different procedures are followed to insert the filaments. For the joints made of the *Caperlan TX4 60µm* lines, the PEI film is first stacked on the top of a paper sheet with graduation as shown in Figure 1a. Afterwards, each filament is positioned at a time and taped at its edges on the PEI film as shown in Figure 1a. This process is repeated on the other side of the PEI film. As an alternative, shown in Figure 1b, a board has been designed with spikes regularly spaced. The filaments are wrapped around the nails, as shown in Figure 1b, to impose a constant and controlled spacing. Once inserted, the filaments are taped along the edge of the PEI film before cutting the filament sections surrounding the nails. This prevents cutting each filament deposited at a time. The process is repeated on both sides of the PEI film, see Figure 1c.

The joints are manufactured by resin transfer moulding in the following sequence. The first five G0926 carbon plies are first laid down in the RTM mould, parallel to one another. The PEI film with the cords on both sides is introduced following the procedure described in the

[3] Data in kg are the supplier data.

previous paragraph. Two 70 mm long, 30µm thick Kapton films (Dupont) are stacked on top of PEI to act as pre-crack for the fracture tests. The five last plies are then deposited. The RTM mould is closed under a pressure of 8 bars. The RTM6 resin is heated inside a piston up to 90°C before being injected at the same temperature in the mould until reaching a pressure of 6 bars. The composite is cured following the optimized cycle for PEI-RTM6 interphase developed by Voleppe et al. (Voleppe et al., 2021). The temperature is increased at a rate of 2°C/min up to 160°C for 90 min. Finally, the temperature is increased up to 180°C at a rate of 2°C/min and the temperature is maintained constant for two hours. Double cantilever beam (DCB) samples are machined in the panels as shown in Figure 2a.

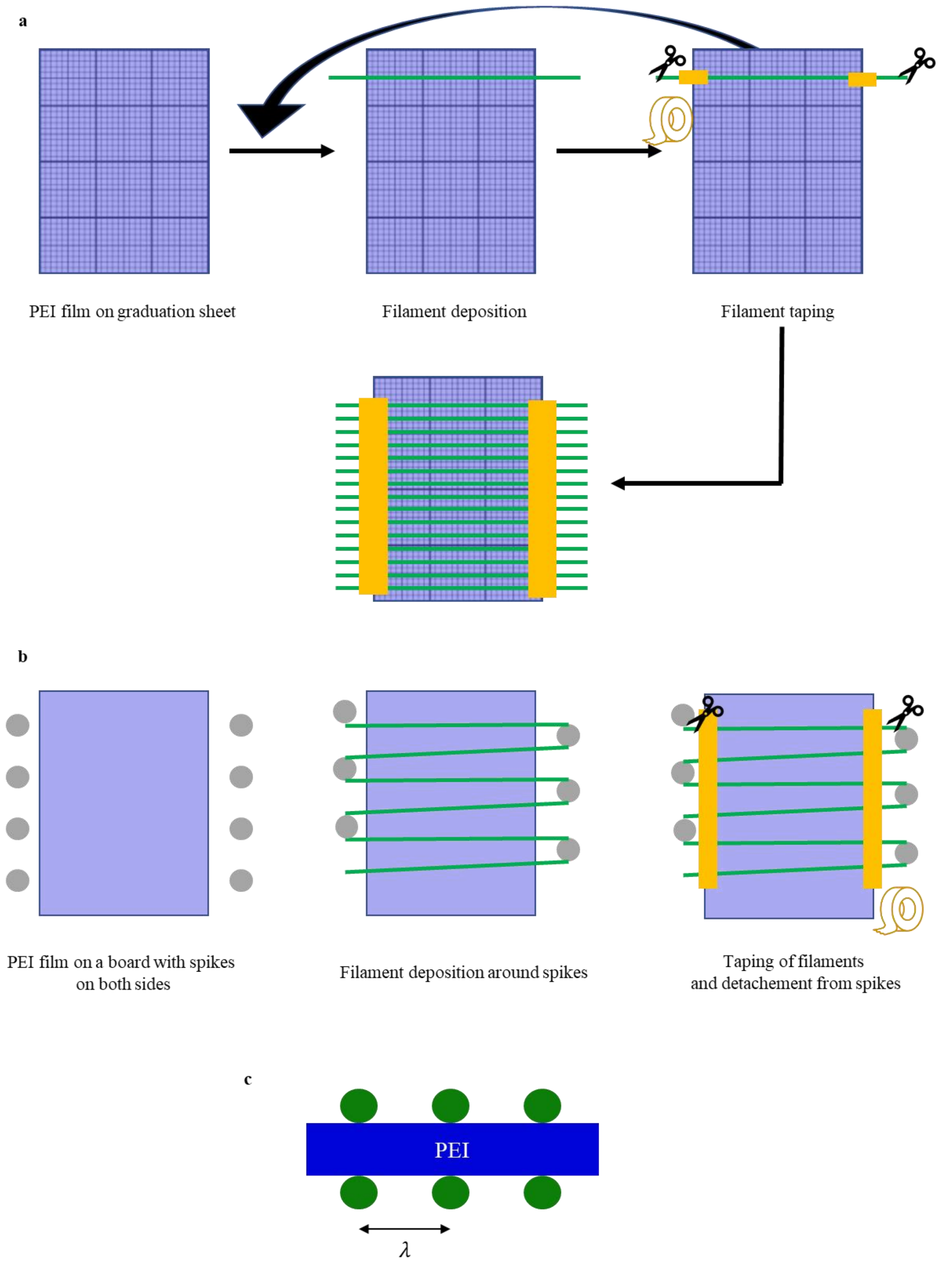

Figure 1: Two methods to insert the filaments: a) filament deposition based on a sheet with graduation and b) filament deposition using a board with spikes spaced by a given λ. c) Final results from the PEI film edge with filaments on both sides of the PEI.

2.3.Mechanical testing

DCB specimens, shown in Figure 2a-b, are machined from the cured panels with a length of 200 mm and a width of 20 mm in such a way that UHMPE filaments are aligned perpendicular to the crack propagation direction (Figure 2c). The 70 mm long Kapton film inserted to create the pre-crack (distance between crack-tip and loading point) corresponds to an initial crack length of 50 mm. The total height of the samples is about 4 mm. The DCB tests are performed following the ISO 25217 standard (ISO, 2014) on a Zwick/Roell machine equipped with a 50 kN loadcell, at constant crosshead speed of 1 mm/min. The machine is located in a ventilated room under constant temperature of 23°C and 50% relative humidity content, respectively. Prior to testing, the edges of the samples are graduated to measure the crack length by taking pictures every 3 seconds with a Canon EOS1400D camera. The mode I toughness G_{Ic} is then computed following the single beam theory (ISO, 2014). Four replicate samples are tested for each condition, except for a spacing of 7 mm for which only one sample is available.

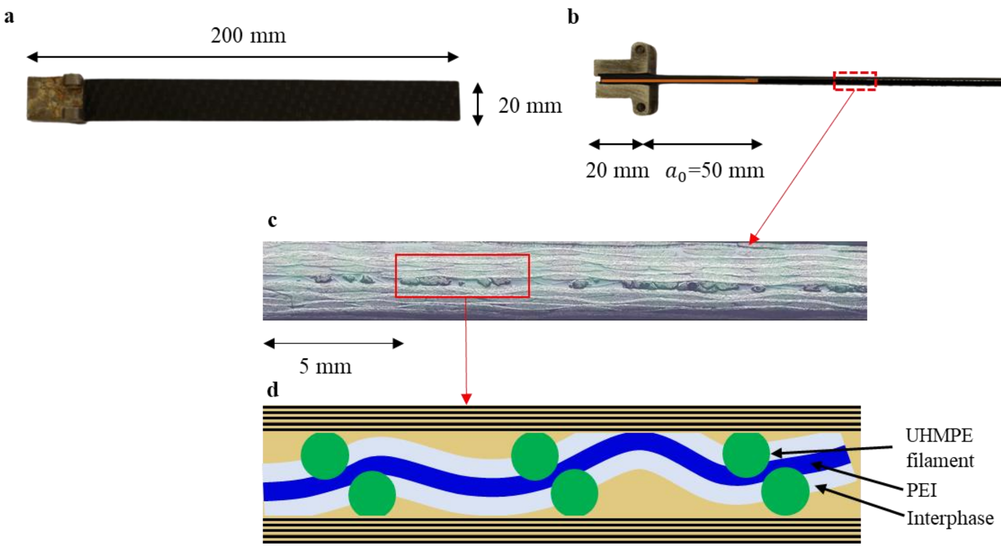

Figure 2: a-b) DCB sample and dimensions from a) the top and b) the side. c) Optical micrograph of the bondline with UHMPE filaments spaced by 1 mm. d) Schematic view of the DCB sample with UHMPE cords.

2.4.Microscopy

A Ultra 55 Field-Emission scanning electron microscope (FEG-SEM) (Zeiss, Germany) under 5 keV and an optical microscopy with a VHX microscope from Keyence are used to perform the fractography analyses. This requires cutting the joints along the crack propagation direction and polishing the cross-section prior to characterization.

3. Analytical model

3.1.Governing equations

An analytical model with a discrete bridging law, similar to the one of Li et al. (Li et al., 2021), has been worked out in order to analyse the effect of filament bridging on the joint toughness. The model parameters consist of the joint toughness in the absence of bridging filaments G_0, the filament spacing λ, the Young's modulus E^f, UTF F^f and radius *r* of the filaments. The material properties and dimensions of the composite adherents enters the problem. The DCB has a width *B*, arm thickness *h* and is made of a material with Young's modulus *E*. The crack has a current length *a*. More precisely, *n* filaments are positioned with spacing λ, hence located at positions L_i (*i*=1, 2, … *n*) as shown in Figure 3. The deflection at position L_i is given by

$$w_i(L_i) = \frac{PL_i^3}{6EI} - \sum_{j=1}^{i} \frac{F_j}{EI}\left(\frac{L_i^3}{6} - \frac{L_j L_i^2}{2}\right) + C_i L_i + D_i \, , \tag{1}$$

where *P* is the applied force, F_j is the force carried by the bridging filament at position L_j while C_i and D_i are two constants (see Supplementary Material 2). If *i* is set to 0, one gets the deflection at the loading point. Solving these equations requires the derivation of a bridging law relating the force applied to the bridging filament located at L_i to the beam deflection at that same position, as worked out in Section 3.2. In addition to these equations, a crack propagation criterion is required. The crack propagates when the crack tip driving force G_{tip} is equal to the toughness of the joint in the absence of bridging filament G_0:

$$G_{tip} = \frac{1}{BEI}\left(Pa - \sum_{j=1}^{n} F_j\left(a - L_j\right)\right)^2 = G_0\,. \tag{2}$$

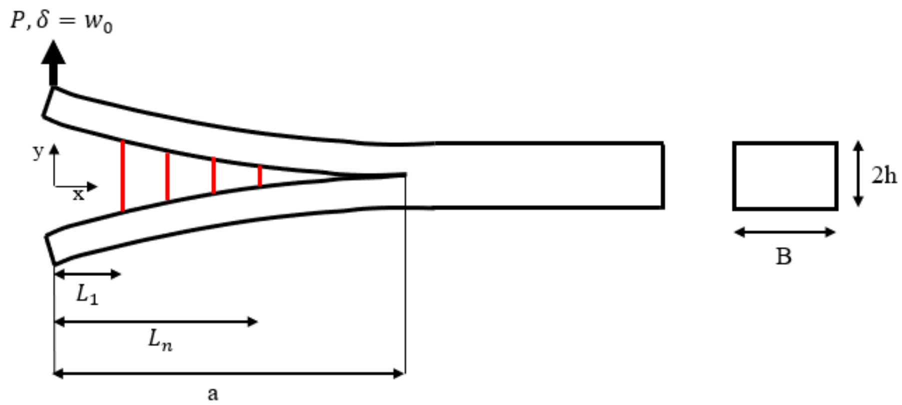

Figure 3: Double cantilever beam configuration with a width B, a height 2h. A crack of length a is bridged by n filaments in its wake, located at the positions L_i.

The unknowns of the problem are thus the deflections at the bridging filament positions, w_i $(i = 1,2, \dots n)$ and the macroscopic force P while the inputs are B, h, E, a, G_0 and the bridging law. The (*n+1*) equations correspond to the *n* equations coming from Eq. (1) and one last equation coming from Eq. (2). A Newton-Raphson method is used with as guess for the k^{th} iteration $X_k = (W_{1k}, W_{2k}, \dots . W_{nk}, P_k)$ and the function to solve is

$$H(X_k) = \begin{pmatrix} W_{1k} - w_1(L_1) \\ W_{2k} - w_2(L_2) \\ \vdots \\ W_{kn} - w_n(L_n) \\ G_{tip} - G_0 \end{pmatrix} = 0\,. \tag{3}$$

Solving this system determines the load P leading to crack propagation ($G_{tip} = G_0$) and the deflections at each bridging ligament. This is repeated for each crack length a in order to predict the corresponding macroscopic load $P(a)$ and overall toughness $G_{Ic}^{tot}(a)$. The numerical algorithm is explained in Supplementary Material 2.

3.2.Bridging law

The bridging law relates the force F_i applied to the filament at position L_i to the deflection at the position of the bridging filament $w_i(L_i)$. The distance between the two DCB arms at the position L_i is equal to $2w_i$. Hence, the bridging law writes $F(2w_i)$. Although the bridging law influences the initial shape of the R-curve, Spearing and Evans (Spearing and Evans, 1992) showed for two different laws, characterized by the same fracture energy (surface area under the curve), the steady-state toughness G_{Ic}^{ss} was similar. The difficulty in the present problem is that there are several possible mechanisms and configurations associated to filament bridging. The filaments are initially in a horizontal position and then get displaced, bent and stretched vertically with a geometry that depends on how the filament remains attached to each side of the joint. Hence, four different laws shown in Figure 4 have been addressed each of them being selected as partly representative of the phenomenology of the bridging configuration observed experimentally (see results later). Law #1 considers that the filaments behave as springs while Law #2 assumes that the filament must first be unfolded before being loaded in tension. Law #3 considers that the filament is attached at the edges at opposite interfaces while law #4 considers a filament attached to the bottom interface, but debonded over a distance *d* and which is bonded to the opposite interface at the middle of the debonded length. The two last laws strongly depend upon the filaments Young's modulus E^f and radius *r*. In all cases, the cords break when the force exerted along the loading axis is equal to the UTF F^f. More details are given in Supplementary Material 2, including an analysis of the impact of the bending versus stretching of the filaments. An influence of the bridging law is found on the results. However, as long as the surface area under the bridging law is constant, a similar toughness is reached and if it is increased, G_{Ic} increases. However, depending on the law, the tensile elongation of the cords differs.

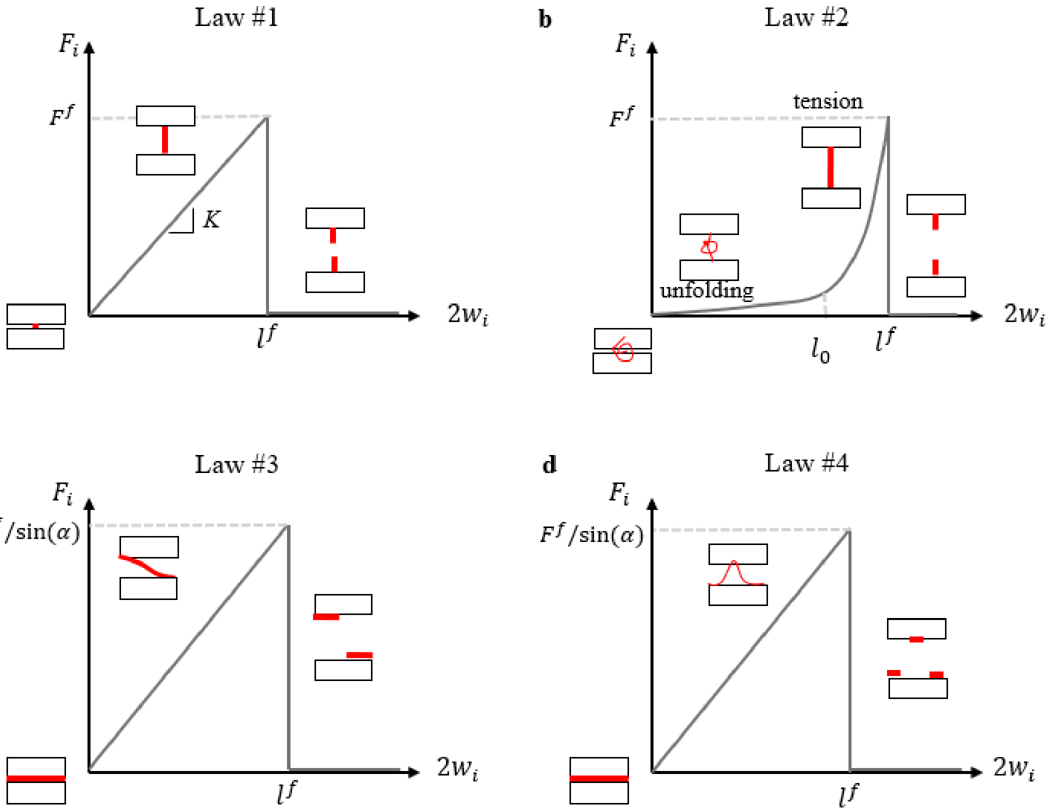

Figure 4: Bridging laws: a) law #1 the filament behaves as a spring, b) law #2 the filament first unfolds before being loaded under tension, c) law #3 the filament is bonded at the edges of the DCB, d) law #4 decohesion takes place over a short distance d while the debonded part adheres to the opposite interface

4. Results

4.1. Influence of the filament spacing on cracking resistance

Figure 5 shows the experimental R-curves extracted from the DCB tests performed on co-cured joints with a 50 µm thick PEI film and threads involving different λ spacing. No matter the spacing, the toughness first increases over a crack propagation distance noted Δa^{ss}, defined in Figure 5b, that varies with λ before reaching a plateau corresponding to the steady-state regime. For a filament spacing of 1 mm, Fig. 5a shows that the steady-state toughness is equal to 760 ± 102 J/m² and the R-effect takes place over a crack length advance Δa^{ss} = 15 mm. If the spacing is increased up to 2 mm, the steady state G_{Ic}^{ss} is about $720 \pm 89\ J/m^2$ and is reached after a crack propagation length about 20 mm. For spacings equal to 5, 7 and 10 mm, the steady-state regime is reached after 40 mm of crack propagation and the steady-state toughness is equal to 430 ± 66, 615 ± 34, 560 ± 99 for each spacing, respectively. One can also define G_{Ic}^{init} for $\Delta a \rightarrow 0$ by linearly extrapolating the results as shown in Fig. 5b. The plain joint toughness G_0 (without bridging filaments) is equal to $285 \pm 89\ J/m^2$, see Supplementary Material 1. The results expressed in terms of normalized quantities G_{Ic}^{init}/G_0 and G_{Ic}^{ss}/G_0 to reveal the degree of toughening are gathered in Figure 5c. Bridging by UHMPE filaments leads to a maximum G_{Ic}^{ss}/G_0 ratio of about 2.7. The toughening effect decreases as the spacing increases.

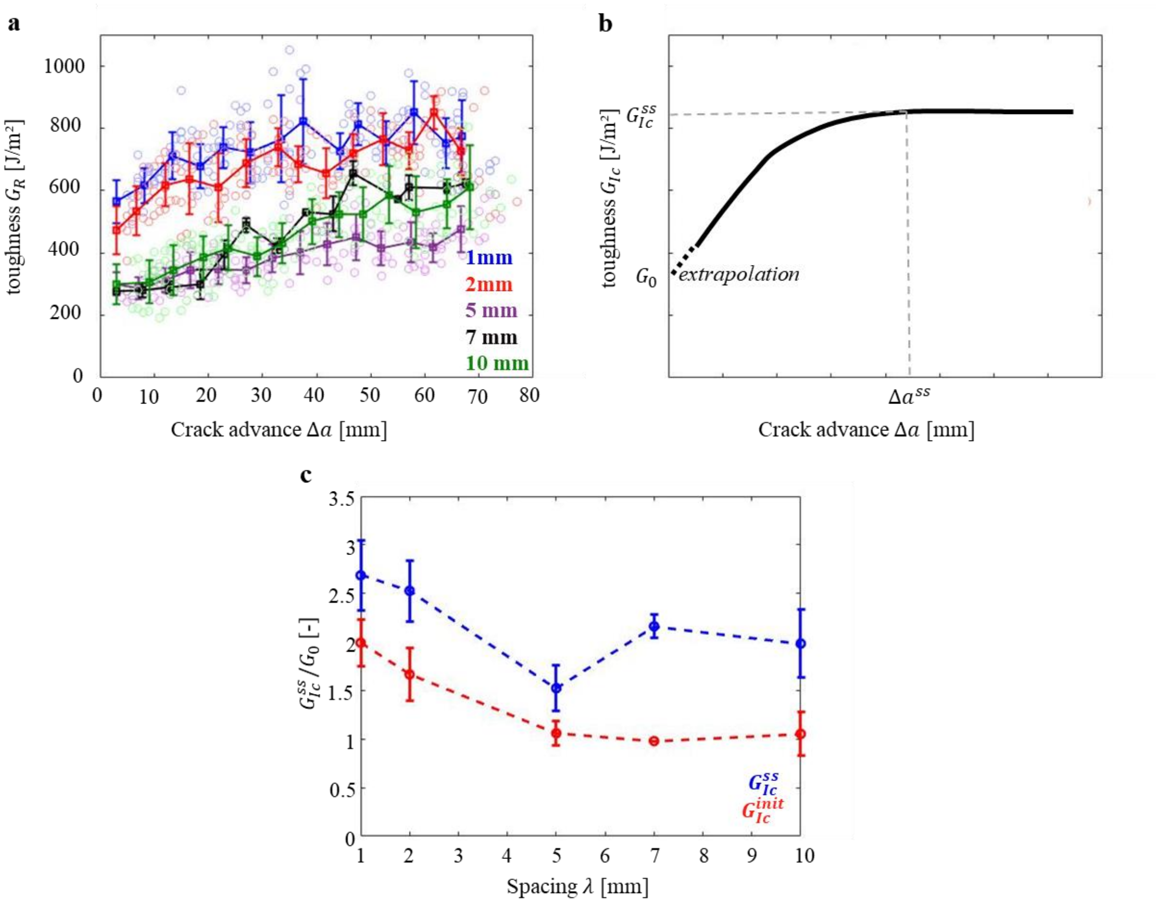

Figure 5: a) R-curves for PEI co-cured composite joints with UHMPE filaments perpendicular to the crack propagation direction spaced by a distance λ equal to 1 (blue), 2 (red), 5 (purple), 7 (black) and 10 (green) mm. b) Scheme of R-curve defining G_{Ic}^{init}, G_{Ic}^{ss} and Δa^{ss}. c) Evolution of steady-state G_{Ic}^{ss} and initiation toughness G_{Ic}^{init} with spacing.

4.2. Influence of filament UTF *on cracking resistance*

Figure 6 presents the R-curves corresponding to the cracking of PEI co-cured composite joints in which cords with different UTFs are inserted. Figure 6a corresponds to joints in which the filaments are spaced by 1 mm while in Figure 6b, they are spaced by 2 mm. For joints containing threads spaced by 1 mm and characterized by a UTF of 56, 81 and 167 N, the steady-state toughness G_{Ic}^{ss} is equal to $560 \pm 141\, J/m^2$, $500 \pm 135\, J/m^2$ and $930 \pm 237\, J/m^2$, respectively. The best toughening effect attained in this work is thus G_{Ic}^{ss}/G_0=3.3 for the 17.2 kg filaments spaced by 1 mm. If the spacing is increased up to 2 mm, 56 N filaments result in a toughness equal to $540 \pm 95\, J/m^2$, the 81 N to a G_{Ic}^{ss} equal to $430 \pm 83\, J/m^2$ and the 167 N to a toughness equal to $495 \pm 187\, J/m^2$. This is summarized in Figure 6c. In the case of the 167 N filaments spaced by 2 mm, a first peak is reached for a crack propagation length of 20 mm with an associated toughness of about $690\, J/m^2$ before a sudden decrease. For the joints made with 1 mm spaced filaments, the toughness tends to increase with the UTF of the cords. When the filaments are spaced by 2 mm, G_{Ic}^{ss} is almost independent of the thread UTF although a slight increase is observed at the beginning of the R-curve with increasing UTF. To conclude, increasing the filament UTF is beneficial to the joint toughness. In addition, the UTF does not influence the distance over which the R-effect is taking place and ranges from 10 to 20 mm in all cases.

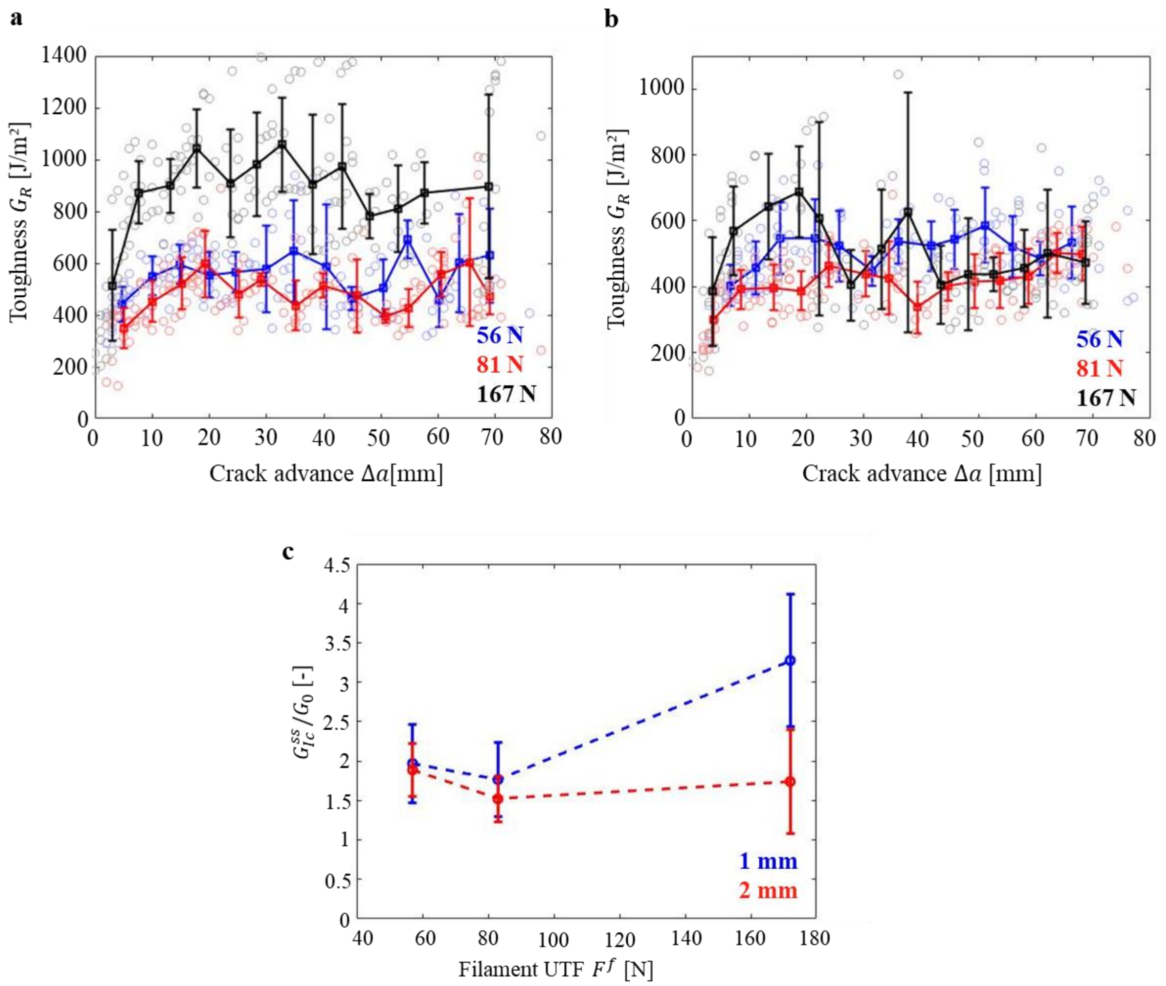

Figure 6: R-curves for PEI co-cured joints containing UHMPE cords of varying UTF: 56 N (blue), 81 N (red) and 167 N (black) spaced by a) 1mm and b) 2 mm. c) Evolution of G_{Ic}^{ss}/G_0 with the filament UTF.

4.3.Fractography

Figure 7 shows the fracture surfaces of specimens with filaments spaced by 1 mm giving interesting indications on the failure mechanisms (results are similar for 2 mm spacing). Figure 7a schematizes the decohesion process of the filaments which might be due to crack propagation between the filament and the composite (Figure 7b) or between the filament and the PEI film (Figure 7c) sometimes takes place. In addition, the crack can propagate along the composite outside of the morphological gradient that forms upon co-curing as revealed by fibre imprints observed in the micrograph of Figure 7b. As for joints without bridging filaments, the crack propagates through the tough PEI film (see Supplementary Material 1 and Figure 7b). In addition, fibre bridging takes place as shown in Figure 7d, originating from a change in crack propagation plane. At a given crack length, along the DCB width, the crack propagates above and below a given cord as shown in Figure 7e and upon loading, the filament breaks as observed on the fracture surfaces in Figure 7f and g. In addition, inserting UHMPE cords results in a wavy PEI film and the presence of the threads induces some degree of crack deflection. Both, crack deflection and bridging induce toughening, but the major contribution most probably arises from crack bridging by the filaments as further justified with the model in Section 5. Figure 7h schematically represents a cross-section of a joint containing cords spaced by at least 5 mm, showing that the PEI film is less wavy. Close to the filaments, mechanisms similar to those shown in Figure 7a are found while between two consecutive threads, the fibres are close to the PEI film and lay thus in the morphological gradient. In these regions, failure mechanisms similar to the one found in joints without bridging filaments are reported in Supplementary Material 1, involving delamination in the PEI-rich zone, propagation along the PEI-rich/epoxy-rich interphase in resin pockets and propagation through the PEI film.

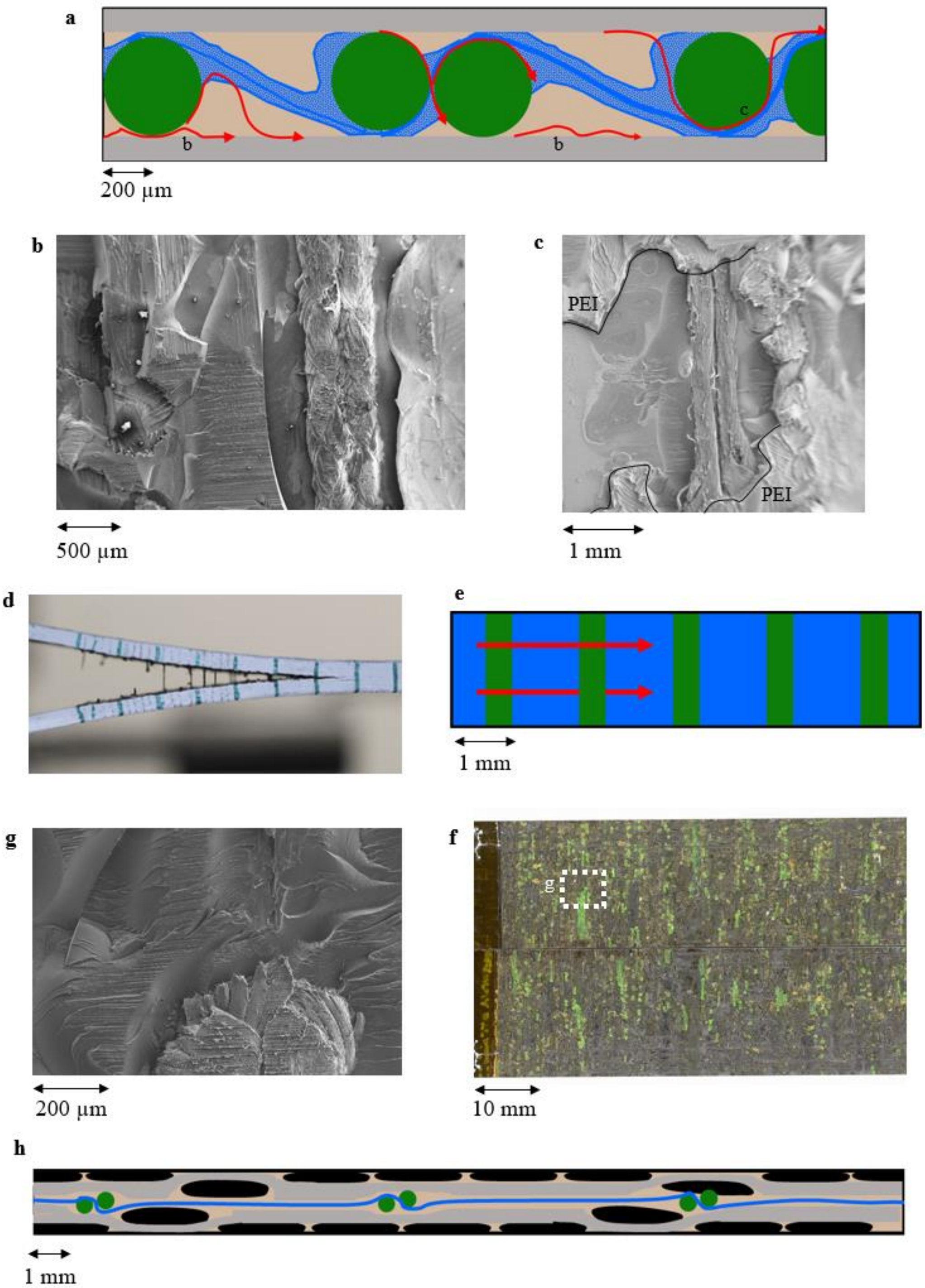

Figure 7: Failure mechanisms in PEI co-cured joints with cords spaced by 1 or 2 mm: a) schematic representation with decohesion of the filament along b) the composite fibres or c) the PEI film with crack propagation through the PEI film. d) DCB picture taking during a test with bridging by the filaments due to e) a crack propagation at both sides of a thread that f-g) breaks upon loading (f optical micrograph and g SEM micrograph). h) Schematic representation along the DCB length for a joint containing cords spaced by 5 mm.

Figure 8 schematizes the bridging mechanism. As shown in Figure 8b, at a given position along the *x* direction, the crack propagates either between the filament and the PEI film or between the filament and the composite. The crack path thus varies along the *z* (width) direction. As shown in Figure 8c-d, this results in the development of bridging filaments. The crack path sometimes changes along the joint width, resulting in many bridging filaments, as shown in Figure 8e, which break upon deformation (Figure 8f), resulting in fracture surfaces with small filament parts as shown in Figure 8 and Figures Figure 7f and Figure 9.

Fractography analyses indicate that the filaments are broken and do not peel from the composite or PEI film surface or are not pulled out of the composite. Regarding the interface between the RTM6 and the UHMPE filament, optical micrographs of unbroken joints do not reveal the formation of any morphological gradient close to the UHMPE filaments. However, the UHMPE filaments correspond to braids in between which the resin can penetrate. Hence, the filament-epoxy interface is quite rough resulting in mechanical interlocking. Regarding the PEI-filament interface, the two materials can hardly interact with each other during curing. However, they are both surrounded by the epoxy resin. Hence, the filaments are embedded in the morphological gradient formed between PEI and RTM6. It is not possible to predict the strength of such interface. Due to the absence of peeling from the composite surface, it is believed that the PEI-filament and RTM6-filament interfaces are strong enough to cause the failure of bridging ligaments under tensile loading.

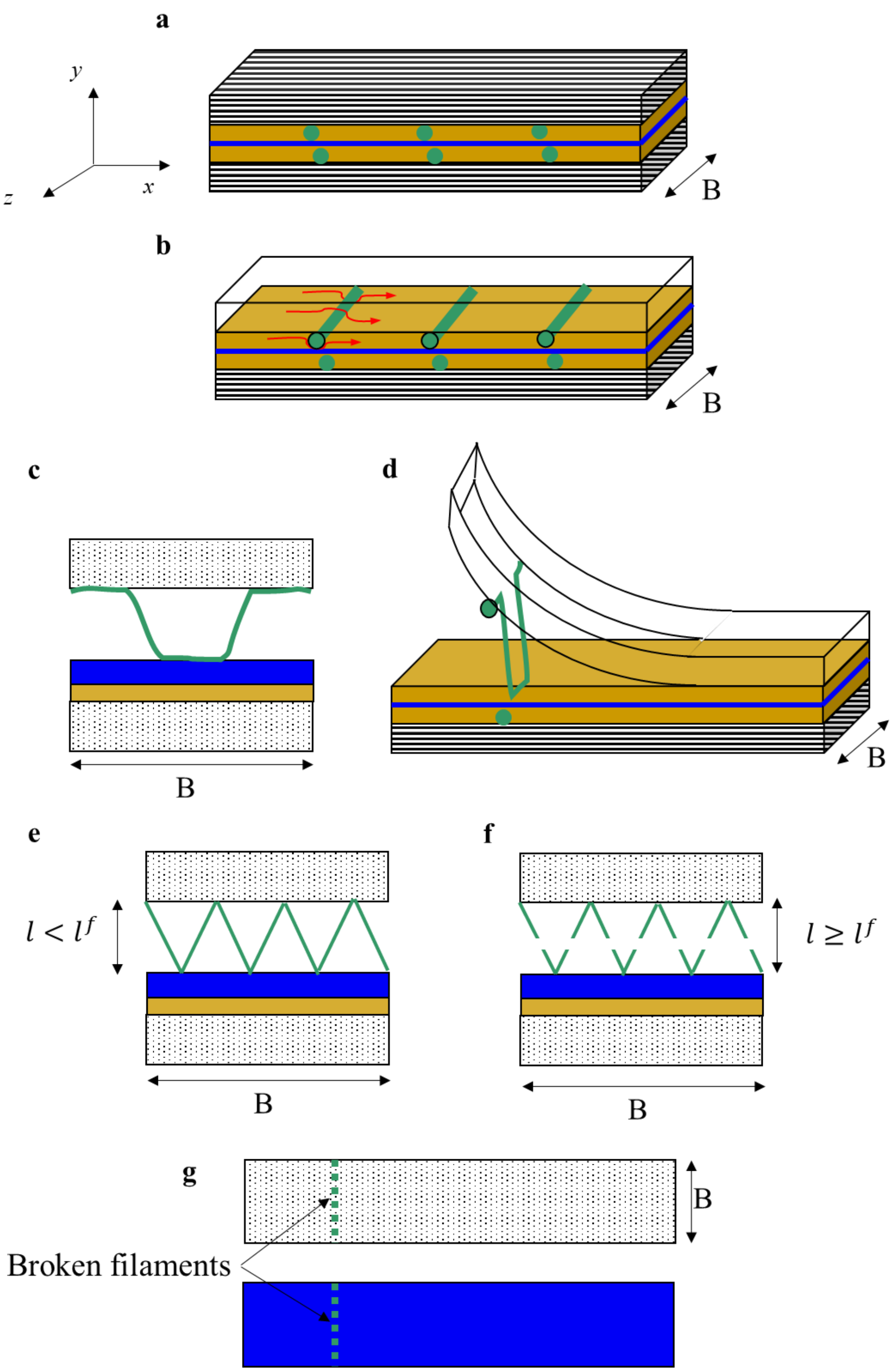

Figure 8 a) Schematic of a joint made of a thermoplastic layer and UHMPE filaments. b-g) Schematic representation of the bridging phenomenon with b) a crack propagating above and under the UHMPE filament for a given $x = L_i$ position resulting in the configuration shown in c) for a view from the open y-z side and d) for a 3D view upon loading. e-f) Generalization to actual joints where one bridging filament can result in several bridging cords e) before filament failure and f) upon failure. g) Schematic of the fracture surface at the composite and PEI film side with bridging filament parts at both sides.

Figure 9 shows the fracture surface of a joint made of 168 N strong filaments spaced by 2 mm. The bottom part exhibits zones with limited number of filaments segments (highlighted in grey), revealing the surface of the composite. In these regions, a limited number of cords act as bridging filament reducing the potential toughening. The same observation is made for all fracture surfaces for this condition, probably explaining the sudden drop in toughness for a crack advance beyond 20 mm in this case (Figure 6b, black line).

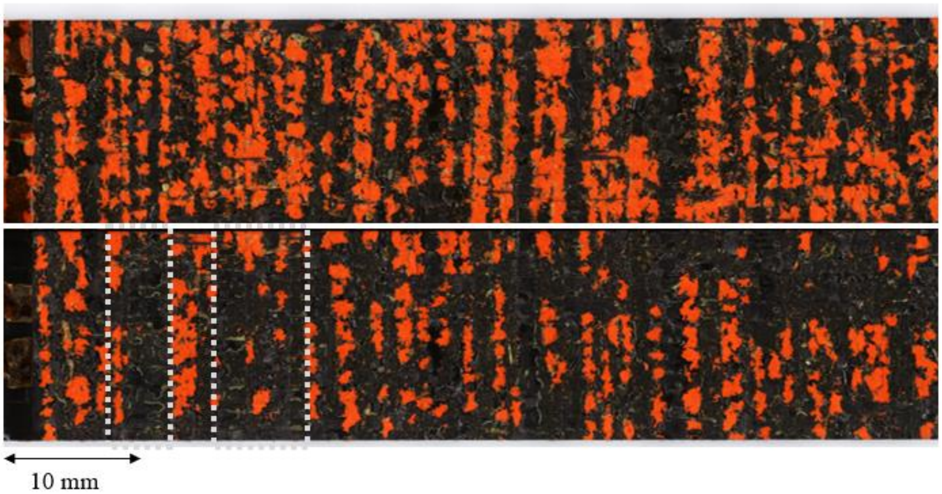

Figure 9: Optical micrograph of the fracture surface of a co-cured composite joint with 167 N strong filaments spaced by 2 mm (orange filaments). The grey regions correspond to zones with a limited number of filaments acting as bridging filaments.

5. Modelling and discussion

The experimental results indicate that the introduction of UHMPE cords in PEI co-cured composite joints results in significant toughening owing to crack bridging. The toughness is increased by a factor of minimum 1.5 up to 3.3 depending on the nature and spacing of the filaments. In H5-satin composites, fibre bridging is known to have only a moderate influence on G_{Ic} when inserting thermoplastic veils leading to toughening factors (G_{Ic}^{ss}/G_0) lower than 2 (Quan et al., 2020). The areal weight is comparable to the one of thermoplastic veils (~10 g/m²) for a joint with filaments spaced by 1 mm (~20 g/m²). The level of toughening found in this work is higher than expected. This also shows that there is room for potentially optimizing thermoplastic veils by controlling the orientation of the fibres. We now use the model presented in Section 3 to investigate deeper the factors influencing this bridging mechanism.

Experimentally, we found that one part of the bridging filament is attached to the top composite part and the other one to the bottom part. Filaments neither pull out of the composite nor peel from the composite surface but fail under tension, indicating that it is the joint toughness that matters and not the toughness of the composite-filament interface nor the PEI-filament interface. As filaments fail under tension, many segments can be observed on the fracture surface as shown in Figure 7f and in Figure 9, indicating that the bridging mechanism can be better assimilated to the behaviour of law #4 described in Section 3.2 (Figure 4d).

5.1.Identification of the model parameters and limitations of the model

The only unknown in the model based on the bridging Law #4 (Figure 4d) is the debonding distance d which is taken next as a fitting parameter. The identification of d is shown in Figure 10 for the 38 N strong cords spaced by 1 and 2 mm. In order to reproduce the experimental results, d must range between 0.25 and 0.5 mm. If now, the 56 N strong cords are considered, d must be set to 0.1 mm, a value similar to the radius of the filament. Hence, in this case, bending of the filaments dominates over tension (Supplementary Material 2). If bending is considered, the results cannot be properly fitted anymore. This may be explained by the low Young's modulus of the threads resulting in large deformations, not captured by the analytical model. The model also neglects potential defects that can be present in the joints.

The distance d is thus an important fitting parameter but it cannot be controlled while depositing the filaments on the PEI film. In addition, the model requires to consider large deformations and tension and bending dominated regimes, including the transition, which is beyond the scope of the present analysis. Consequently, in order to discuss the influence of the spacing and UTF on the joint fracture toughness, the Law #1 will be used.

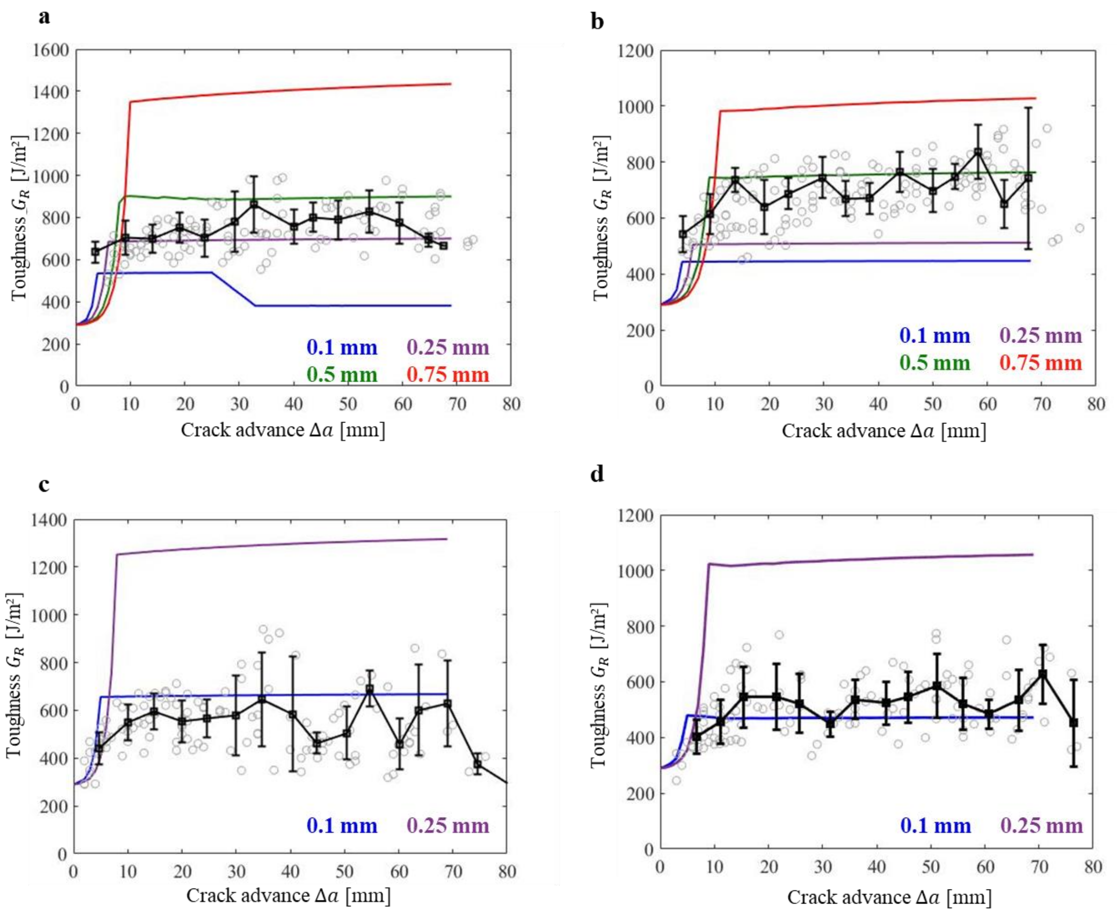

Figure 10: Fitting of experimental results (grey dots and dark line) using Law #4 with different debonding distances d for a) 38 N – 1 mm, b) 38 N – 2 mm, c) 56 N – 1mm and d) 56 N – 2 mm

With Law #1, the fitting parameter is no longer d but the tensile elongation of the filament l^f. Although this law does not represent well the configuration of the physical bridging mechanism, it is possible, for each condition, to determine the l^f values so that the predicted joint toughness matches the experimental G_{Ic}^{ss}. The tensile elongation l^f is determined for the joints with 38 N strong filaments spaced by 1, 2, 5, 7 and 10 mm as shown in Figure 11. Ideally, l^f, as d with Law #4, should keep the same value for all conditions. However, for the 38 N strong cords, values of l^f ranging between 0.4 and 0.6 mm are found to fit the results for $\lambda = 1$ mm while for $\lambda = 2$ mm, l^f must be set with a value between 0.7 mm and 1 mm. Using values for λ ranging from 0.5 to 1.5 mm allows capturing the G_{Ic} of joints with filaments spaced by 5, 7 and 10 mm, but, as with Law #4, the distance over which the R-effect (Δa^{ss}) takes place is then not well predicted. This may arise from a distribution of tensile elongation of the cords as they can debond over different lengths with wide variations. For the filaments characterized by a UTF of 56, 81 and 167 N and λ set to 1 and 2 mm, l^f values ranging between 0.1 et 0.5 mm reproduce the results, except if the UTF is 56 N and λ is set to 2 mm, a condition for which l^f must range between 0.7 and 1 mm (see Supplementary Material 3).

By fitting the experimental results with Law #1, it is found that for the joints for which the filaments have been manually positioned, l^f and d are larger compared to the joints manufactured by inserting the threads using the board with spikes. Placing the cords using the board results in a higher tension in the filaments prior to bonding. The initial tension in the threads may thus have an influence, but this parameter is difficult to control. In summary, all comments made up to this point indicate that the present model thus involves several restricting assumptions and can only be considered as semi-quantitative, although sufficient to discuss next some key trends.

Fine tuning the value of l^f allows fitting the steady-state toughness. However, it is observed in Figures 10, 11, S3.1 and S3.2 that the initial shape of the R-curve (rising part) predicted by the model does not match the experimental response. The experimental response is similar to what is predicted when assuming fibre pull-out, associated with a linearly decreasing bridging law. However, no evidence of fibre pull-out could be seen during the experiments or on the fracture surfaces. In addition, a softening law results in convergence issues. The difference in shape could also come from the fact that experimentally, all filaments do not break at the same l^f and there is thus a distribution of tensile elongation, influencing the results while the model only considers a single value of l^f. Considering a single value for l^f, Spearing and Evans (Spearing and Evans, 1992) showed that, as long as the energy required to break a ligament is the same, the steady-state toughness is not affected by the bridging law shape. The purpose of the actual model is to determine the influence of the bridging properties and the filament spacing on the steady-state toughness, the shape of the bridging law is of minor importance.

The influence of the spacing and of the UTF is discussed now by only considering Law #1 and keeping l^f constant but using different values within the identified spectrum. The goal is thus to unravel the influence of the spacing (section 5.2) and of the UHMPE filament UTF (section 5.3) in order to guide further optimization of the joint toughness (section 5.6).

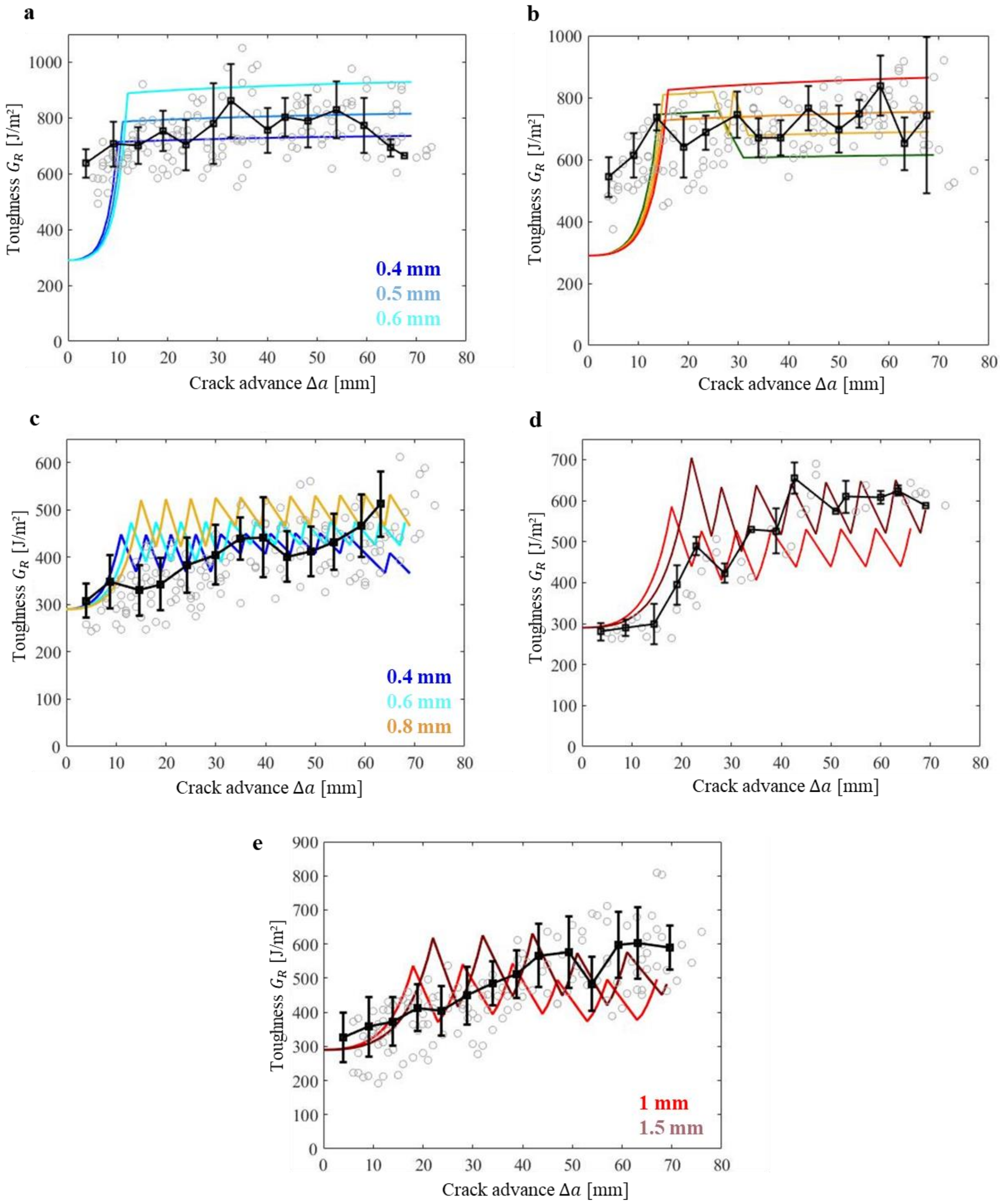

Figure 11: Identification of l^f on experimental results (grey dots and dark line) using the bridging law #1 for different spacings by adjusting the tensile elongation: a) 1mm, b) 2mm, c) 5 mm, d) 7 mm, e) 10 mm.

5.2.Influence of filament spacing

Figure 12a shows that the maximum toughness G_{Ic}^{max} decreases as the spacing between the cords decreases in agreement with the experimental results. Above a spacing λ_{c1}, a stick-slip behaviour (Figure 12c, $\lambda = 4$ mm) is predicted because when one thread breaks, the crack advances but without additional filament introduced behind the crack tip. This results in a saw-tooth R-curve as shown in Figure 12c (dashed lines). Above a spacing λ_{c2}, the spacing does no longer influence the maximum and minimum G_{Ic} attained during crack propagation and the minimum G_{Ic} (G_{Ic}^{min}) is equal to G_0. For the threads characterized by a tensile elongation of 0.25 mm and 1 mm, $G_{Ic}^{min} = G_0$ when the spacing between the threads is equal to 9 and 19 mm, respectively. As shown in Figure 12b, $G_{Ic}^{min} = G_0$ occurs when the bridging zone length l_b is equal to λ. The bridging zone length corresponds to the zone comprised between the first intact filament behind the crack tip and the crack tip. If λ is lower than l_b, there is always at least one filament acting as bridging filament so that $G_{Ic}^{min} > G_0$. If $\lambda > \lambda_{c2}$, stick-slip is also found as shown in Figure 12c with the maximum toughness corresponding to the toughness in the presence of one filament and the minimum one to the joint toughness without bridging ($G_{Ic}^{min} = G_0$). In this case, any increase of spacing does not affect the toughness but as λ increases, the frequency at which a peak toughness is reached decreases, reducing the number of toughening events. For values of l^f up to 5 mm, λ_{c1} is not affected by l^f and is equal to 2 while λ_{c2} increases as l_f increases as it increases l_b.

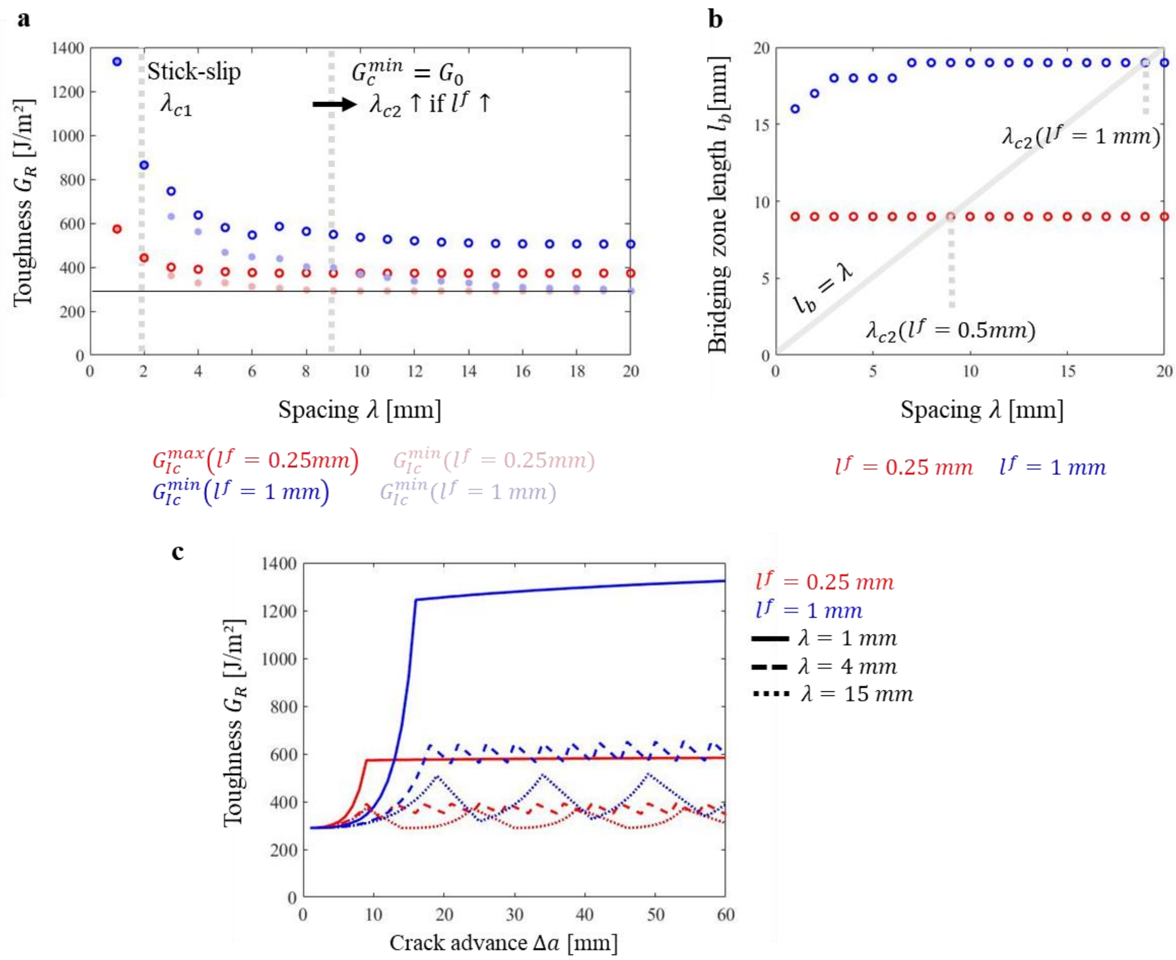

Figure 12: Influence of the filament spacing on the joint toughness and response of the joint for two tensile elongations of the filaments equal to 0.5 and 1 mm: a) evolution of toughness with spacing, b) evolution of the bridging zone length with the spacing and c) R-curves for spacings of 1, 4 and 15 mm.

5.3.Influence of the filament UTF

The UTF of the filament can be increased by changing the material, by triggering bridging filaments acting in parallel (several filaments at each position L_i) (Li et al., 2021) and/or by increasing the diameter of the filament. For a given spacing and tensile elongation of the filaments, increasing the UTF generally results in higher toughness, but with exceptions as shown in Figure 13a. This arises from the fact that as the UTF increases, the bridging zone length progressively decreases. For two filaments of similar UTFs such that $F^{f1} < F^{f2}$, it is possible to have $l_b^1 > l_b^2$ resulting in a more pronounced toughening effect for fibres of UTF F^{f1}. This is illustrated in Figure 13c. In addition, the toughening effect resulting from an increase of UTF also depends on their tensile elongation. The toughening effect is enhanced with increasing l^f. Figure 13a shows that although the spacing between the filaments is set to 1 mm, some conditions result in a maximum and minimum toughness. A R-curve corresponding to such case is shown in Figure 13d. As the crack advances, the deflection at a distance l_b slightly increases and may exceed the tensile elongation of the filament, then reducing the bridging zone length and the toughness. For a given tensile elongation of 0.5 mm, the combined influence of UTF and spacing is shown in Figure 13b. Increasing the UTF results in an increase of λ_{c2}.

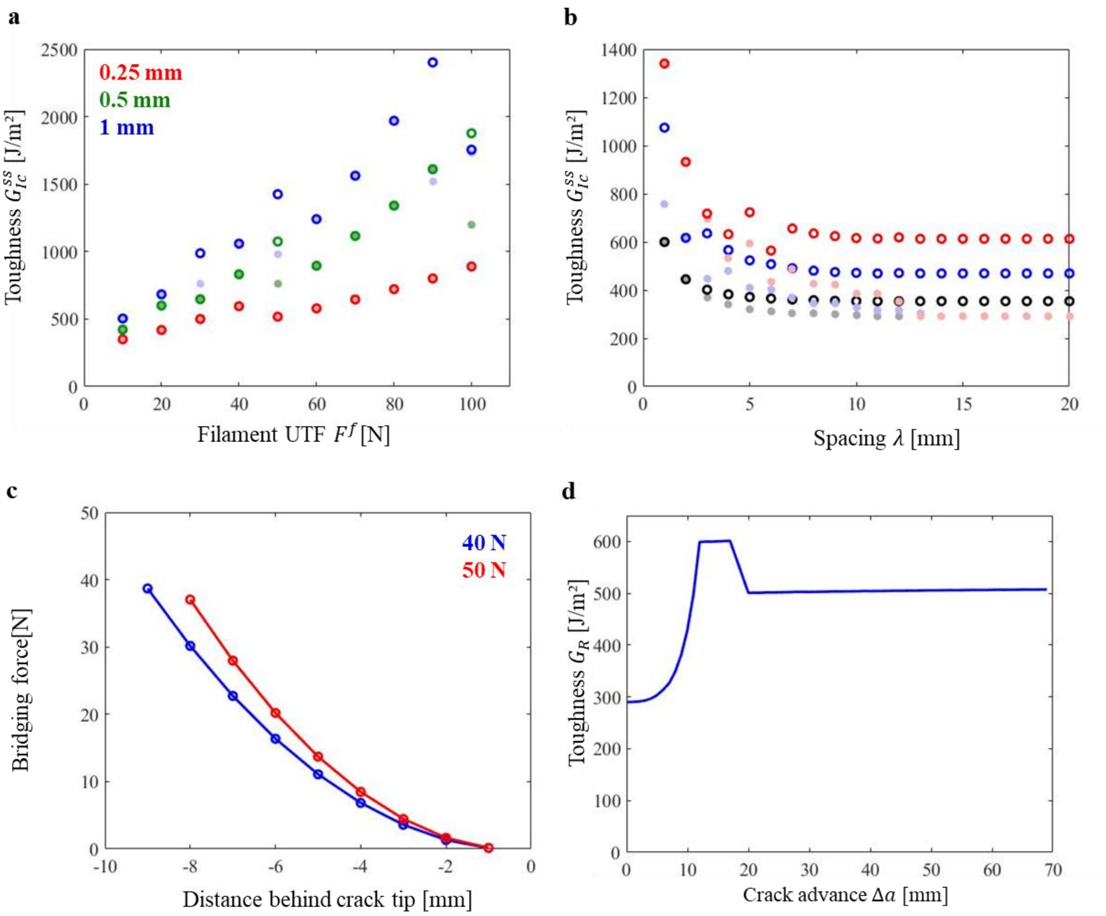

Figure 13: Influence of the UTF *of the UHMPE threads on toughness: a) spacing of 1 mm and different elongations (0.25, 0.5 and 1 mm), b) combined influence of* UTF *and spacing, c) Increase in* UTF *with a decrease in bridging zone length reducing the toughness (lambda 1 mm, l^f 0.5 mm), d) R-curve exhibiting a local stick-slip behaviour as the bridging zone length is suddenly reduced.*

5.4. Influence of the tensile elongation of the filaments

The influence of the tensile elongation has been previously discussed with the UTF and filament spacing. An increase in tensile elongation results in an increase in toughness. However, as the tensile elongation is increased, the distance over which the R-effect takes place increases, delaying the attainment of the maximum toughness. In addition, by decreasing the tensile elongation, the toughening effect resulting from the smaller spacing and UTF increase is reduced. For the 56, 81, 167 N strong cords, using bridging Law #1, the tensile elongation is assumed to be around 0.1 and 0.2 mm (Supplementary Material 3), explaining why the toughening effect resulting from an increase in tensile UTF is not properly captured experimentally.

5.5. Influence of the joint toughness without bridging filaments

Regarding the influence of the initial joint toughness, several comments can be made. First, the contribution of bridging $(G_{Ic}^{ss} - G_0)$ to the toughness is independent on G_0 as shown in Figure 14a. This means that the energy released during crack propagation corresponding to bridging and thus filament breaking is independent of G_0. Let's consider, joints of initial toughness G_{01} and G_{02} such that $G_{01} < G_{02}$ and thus $l_{b1} > l_{b2}$. If in both cases, the steady-state is reached and the crack advances by 1 mm assuming $\lambda = 1$ mm. As the crack propagates, the first filament of the bridging zone breaks for both joints, associated with a release of energy equal to $l^f F^f/2$. As the change in potential energy due to bridging is independent of G_0, the contribution of bridging $(G_{Ic}^{ss} - G_0)$ is also independent of G_0 and is equal to $\frac{l^f F^f}{2B\Delta a}$ as shown in Figure 14a. This indicates that the bridging contribution increases as the energy required to break one filament increases, in agreement with the previous results regarding l^f and F^f. However, relatively speaking, the toughening effect G_{Ic}^{ss}/G_0 decreases as the initial toughness decreases as shown in Figure 14b. Indeed, for a bare joint without bridging filaments, if G_0 increases, the beam deflection at a distance x from the crack tip increases. Hence, when the filaments are inserted, for low values of G_0, the distance between the two DCB arms at a position L_i does not exceed l^f while this value is well exceeded for larger values of G_0. Hence, the bridging zone length decreases as G_0 increases as shown in Figure 14c, reducing the energy dissipated in the bridging zone. Finally, it is important to note that G_0 only slightly affects the distance over which the R-effect takes place.

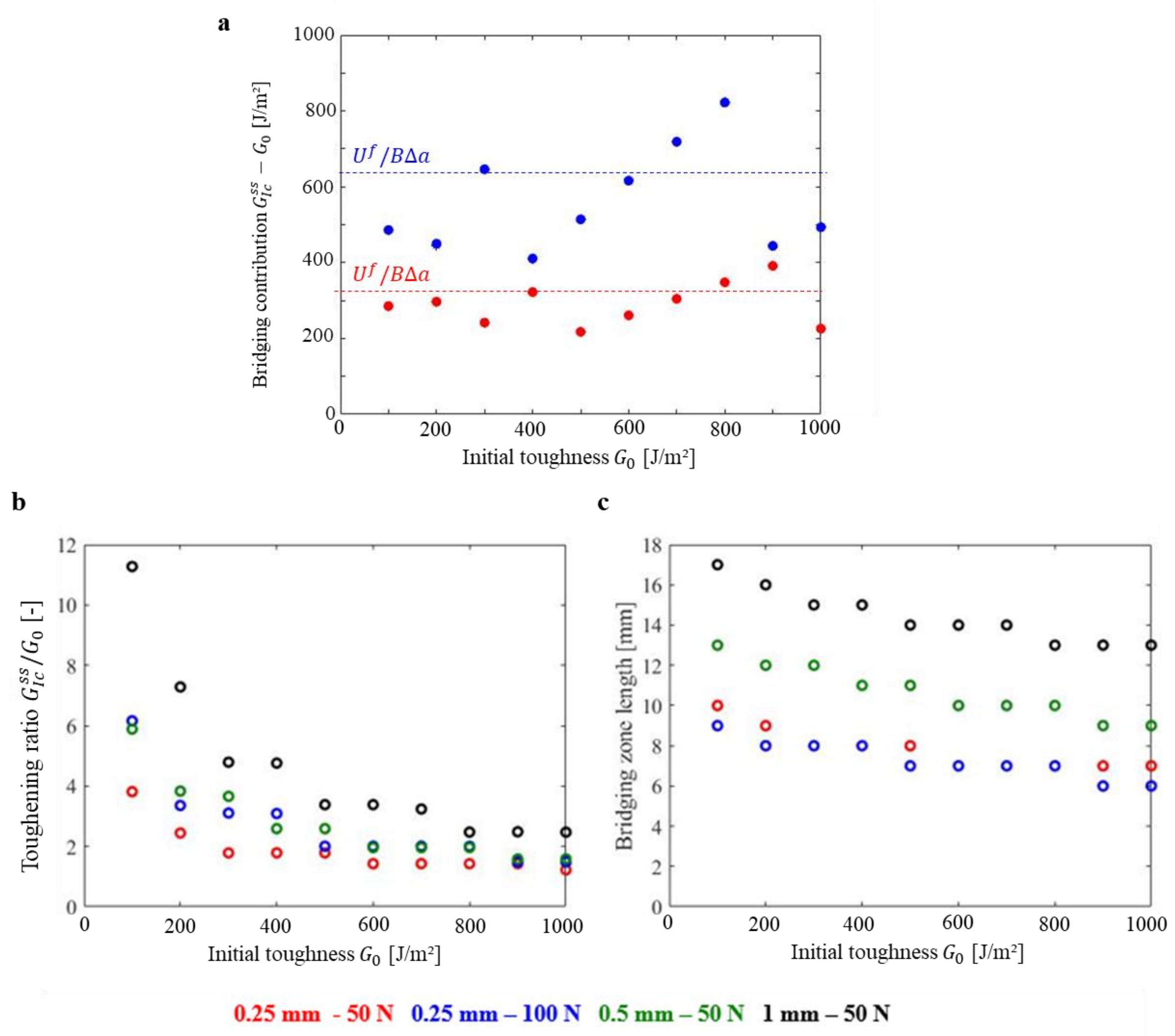

Figure 14: Influence of G_0 on a) the bridging contribution $G_{Ic} - G_0$, b)on the relative toughening effect G_{Ic}/G_0 and c) the bridging zone length l_b. λ mm is set to 1 mm while F^f and l^f are varied.

In Supplementary Material 1, the relative toughening effect is shown to be slightly larger in joints with a 175 µm PEI film than in joints with a 50 µm thick film, in agreement with the analytical model results indicating a decrease of G_{Ic}^{ss}/G_0 as G_0 decreases. However, the bridging contribution is about 470 J/m² with the 50 µm thick film and about 320 J/m² for the 175 µm thick film, and this difference can only be explained by some process variability or by slight changes of failure mechanisms between the two joints.

5.6.Optimizing joints with architected bridging

The optimization of the joint properties depends on the architecture, which requires determining the influence of the architecture parameters (geometry and properties) on several joint properties including, among others, toughness, shear strength, shear stiffness, and tensile strength. In the present study, only the influence of the architecture on the mode I toughness has been investigated. Hence, it is solely possible to discuss the optimal architecture in a case where a crack is subjected to peel stresses and that is sufficiently long such that toughness dominates the problem owing to scale effects. The critical crack length above which toughness dominates and not the strength depends on the thickness of the bondline, the process zone size ahead of the crack tip and the elastic mismatch between the adherents and bondline materials (Van Loock et al., 2019).

The influence of the bridging filament properties, distribution and the initial joint toughness have been investigated in the previous sections. Increasing the UTF and the tensile elongation of the filaments and decreasing the spacing between the filaments results in an improved toughening effect (G^{ss}/G_0). The UTF can be increased by (i) changing the filament materials for a stronger material, (ii) increasing the filament or (iii) by triggering bridging filaments acting in parallel. The toughening effect is dependent on G_0.

To consider the influence of spacing, filament properties, adherent properties and dimensions, it is possible to derive a non-dimensional number that will be referred to as the relative toughening effect, by analogy to the brittleness number derived by Carpinteri and his co-workers (Accornero et al., 2022; Carpinteri, 1984) for reinforced concrete. The derivation of the relative toughening effect number is given in Supplementary Material 4 which leads to

$$N^p = \frac{F^f l_b^2}{B\lambda\sqrt{G_0 E h^3}} \quad (4)$$

with the bridging zone l_b increasing if l^f, E, h or B increases or G_0 or a decrease. It indicates that increasing F^f, l^f, E, B or h results in a higher toughening effect while a decrease in λ results in an improvement of the toughening effect, in agreement with the experimental and analytical model results for a given G_0. This number also indicates that for tougher joints, bridging is less efficient to toughen the joint in terms of relative toughening effect although the steady-state toughness will be higher. In addition, it is only valid if the filaments fail under tension.

It is important to note that regarding the tensile elongation, it increases the steady-state toughness of the joint but also the distance over which the R-effect takes place, Δa_{ss}. Hence, in some case, for short crack propagation distance, if one considers two joints made of the same bridging filaments but with different elongation, the joint with the less ductile filaments can be tougher than the one with the ductile filaments, as shown in Figures 11 and 12c. The effect of l^f on Δa^{ss} is not taken into account in the derivation of the relative toughening effect number N^p. For long crack propagation distances, the joint with ductile filaments (larger l^f) is the toughest as suggested by Equation 4. Consequently, the design of the joint depends upon the maximum allowable crack length and N^p gives the right trend if for all joints compared to each other $a > l_b$.

It is also important to note that the optimum design will also depend on the influence of the above-mentioned parameters on other properties of the joint such as its shear strength and shear stiffness. Such an investigation is left for further work with the goal to select the best joint design by following a rational selection methodology as presented in the study by van Innis and Pardoen (van Innis and Pardoen, 2023).

6. Conclusion

Co-curing of composites with an adhesive is an attractive alternative to secondary bonding, but it often involves lower joint toughness. As a solution, the adhesive can be replaced by a thermoplastic film such as PEI. The joint toughness is then enhanced compared to composite delamination for composites manufactured based on pre-pregs. However, when the same co-curing is performed using a resin transfer moulding process, a toughness lower than the composite delamination toughness is found requiring the adoption of an extra toughening strategy. Here, crack bridging has been triggered by inserting UHMPE filaments at both sides of the PEI film resulting in an improvement of the toughness by a factor up to 3.3. Joints with UHMPE filaments are thus characterized by a toughness significantly larger than the delamination toughness of the composite and compete, depending on the design parameters, with classical adhesive joints.

The toughness of the joint is controlled by the spacing between the filaments, the failure load and the tensile elongation of the filaments. A smaller spacing and high failure load of the filaments improves the fracture toughness. Increasing the tensile elongation of the ligaments also results in larger toughness, but it requires longer crack advances to reach the steady-state toughness. Hence, for small crack propagation length, joints with less ductile filaments can be tougher than joints with ductile filaments. Consequently, the joint design must consider the maximum allowable crack extension, and the level of toughness required upon a certain crack propagation distance to fulfil the mechanical requirements. If the crack is allowed to only extend over a small distance, it is preferable to increase the bridging filament failure load by changing material, increasing the filament radius or have filaments acting in parallel than increasing the tensile elongation. If the crack extends without restriction, increasing the tensile elongation of the filament is an option, however, difficult to control experimentally. This optimization could be performed in the context of a rigorous adhesive selection strategy following (van Innis and Pardoen, 2023).

Acknowledgments

C.vI. is a FRIA grantee of the Fonds de la Recherche Scientifique de Belgique - FNRS and gratefully acknowledges their support. The authors gratefully acknowledge the Sonaca for the discussions and the supply of the carbon fibres and the RTM6 resin.

Data availability

The data that support the findings of this study are available on request from the corresponding author C.vI.

Competing interests

All authors declare that they have no other competing interests.

References

Accornero, F., Rubino, A., Carpinteri, A., 2022. Post-cracking regimes in the flexural behaviour of fibre-reinforced concrete beams. Int. J. Solids Struct. 248, 111637. https://doi.org/10.1016/j.ijsolstr.2022.111637

Anders, M., Zebrine, D., Centea, T., Nutt, S., 2017. In Situ Observations and Pressure Measurements for Autoclave Co-Cure of Honeycomb Core Sandwich Structures. J. Manuf. Sci. Eng. Trans. ASME 139, 1–9. https://doi.org/10.1115/1.4037432

Anders, M., Zebrine, D., Centea, T., Nutt, S.R., 2019. Process diagnostics for co-cure of sandwich structures using in situ visualization. Compos. Part A Appl. Sci. Manuf. 116, 24–35. https://doi.org/10.1016/j.compositesa.2018.09.029

Athanasiadis, A.E.F., Dias, M.A., Budzik, M.K., 2021. Can confined mechanical metamaterials replace adhesives? Extrem. Mech. Lett. 48, 101411. https://doi.org/10.1016/j.eml.2021.101411

Bascom, W.D., Cottington, R.L., Jones, R.L., Peyser, P., 1975. The fracture of epoxy- and elastomer-modified epoxy polymers in bulk and as adhesives. J. Appl. Polym. Sci. 19, 2545–2562. https://doi.org/10.1002/app.1975.070190917

Bertholet, Y., Olbrechts, B., Lejeune, B., Raskin, J.P., Pardoen, T., 2007. Molecular bonding

aided by dissipative inter-layers. Acta Mater. 55, 473–479. https://doi.org/10.1016/j.actamat.2006.08.036
Brito, C.B.G., Sales, R.C.M., Donadon, M. V., 2020. Effects of temperature and moisture on the fracture behaviour of composite adhesive joints. Int. J. Adhes. Adhes. 100, 102607. https://doi.org/10.1016/j.ijadhadh.2020.102607
Carpinteri, A., 1984. Stability of Fracturing Process in RC Beams. J. Struct. Eng. 110, 544–558. https://doi.org/10.1061/(asce)0733-9445(1984)110:3(544)
Carpinteri, A., Accornero, F., 2018. Multiple snap-back instabilities in progressive microcracking coalescence. Eng. Fract. Mech. 187, 272–281. https://doi.org/10.1016/j.engfracmech.2017.11.034
Cartié, D.D.R., Troulis, M., Partridge, I.K., 2006. Delamination of Z-pinned carbon fibre reinforced laminates. Compos. Sci. Technol. 66, 855–861. https://doi.org/10.1016/j.compscitech.2004.12.018
Cheng, C., Zhang, C., Zhou, J., Jiang, M., Sun, Z., Zhou, S., Liu, Y., Chen, Z., Xu, L., Zhang, H., Yu, M., 2019. Improving the interlaminar toughness of the carbon fiber/epoxy composites via interleaved with polyethersulfone porous films. Compos. Sci. Technol. 183. https://doi.org/10.1016/j.compscitech.2019.107827
Cordisco, F.A., Zavattieri, P.D., Hector, L.G., Carlson, B.E., 2016. Mode I fracture along adhesively bonded sinusoidal interfaces. Int. J. Solids Struct. 83, 45–64. https://doi.org/10.1016/j.ijsolstr.2015.12.028
Cox, B.N., Marshall, D.B., 1994. Concepts for bridged cracks in fracture and fatigue. Acta Metall. Mater. 42, 341–363. https://doi.org/10.1016/0956-7151(94)90492-8
Cox, B.N., Marshall, D.B., 1991. The determination of crack bridging forces. Int. J. Fract. 49, 159–176. https://doi.org/10.1007/BF00035040
Deng, S., Djukic, L., Paton, R., Ye, L., 2015. Thermoplastic-epoxy interactions and their potential applications in joining composite structures - A review. Compos. Part A Appl. Sci. Manuf. 68, 121–132. https://doi.org/10.1016/j.compositesa.2014.09.027
Dépinoy, S., Strepenne, F., Massart, T.J., Godet, S., Pardoen, T., 2019. Interface toughening in multilayered systems through compliant dissipative interlayers. J. Mech. Phys. Solids 130, 1–20. https://doi.org/10.1016/j.jmps.2019.05.013
Farooq, U., Heuer, S., Teuwen, J., Dransfeld, C., 2021. Effect of a Dwell Stage in the Cure Cycle on the Interphase Formation in a Poly(ether imide)/High Tg Epoxy System. ACS Appl. Polym. Mater. 3, 6111–6119. https://doi.org/10.1021/acsapm.1c00956
Farooq, U., Sakarinen, E., Teuwen, J., Alderliesten, R., Dransfeld, C., 2023. Synergistic Toughening of Epoxy through Layered Poly (ether imide) with Dual-Scale Morphologies. Appl. Mater. Interfaces 15, 53074–53085. https://doi.org/10.1021/acsami.3c10096
Farooq, U., Teuwen, J., Dransfeld, C., 2020. Toughening of epoxy systems with interpenetrating polymer network (IPN): A review. Polymers (Basel). 12. https://doi.org/10.3390/POLYM12091908
Hedvard, M.L.S., Dias, M.A., Budzik, M.K., 2024. Toughening mechanisms and damage propagation in Architected-Interfaces. Int. J. Solids Struct. 288, 112600. https://doi.org/10.1016/j.ijsolstr.2023.112600
Heide-Jørgensen, S., Budzik, M.K., 2018. Effects of bondline discontinuity during growth of interface cracks including stability and kinetic considerations. J. Mech. Phys. Solids 117, 1–21. https://doi.org/10.1016/j.jmps.2018.04.002
Heide-Jørgensen, S., Budzik, M.K., Turner, K.T., 2020. Mechanics and fracture of structured pillar interfaces. J. Mech. Phys. Solids 137, 103825. https://doi.org/10.1016/j.jmps.2019.103825
Heide-Jørgensen, S., Teixeira de Freitas, S., Budzik, M.K., 2018. On the fracture behaviour of

CFRP bonded joints under mode I loading: Effect of supporting carrier and interface contamination. Compos. Sci. Technol. 160, 97–110. https://doi.org/https://doi.org/10.1016/j.compscitech.2018.03.024
Hexcel, 2018. HexFlow ® RTM6, Product Data Sheet.
Hoffmann, J., Scharr, G., 2018. Mode I delamination fatigue resistance of unidirectional and quasi-isotropic composite laminates reinforced with rectangular z-pins. Compos. Part A Appl. Sci. Manuf. 115, 228–235. https://doi.org/10.1016/j.compositesa.2018.10.013
Invernizzi, S., Trovato, D., Hendriks, M.A.N., Van de Graaf, A. V., 2011. Sequentially linear modelling of local snap-back in extremely brittle structures. Eng. Struct. 33, 1617–1625. https://doi.org/10.1016/j.engstruct.2011.01.031
ISO, 2014. ISO25217 Adhesives — Determination of the mode 1 adhesive fracture energy of structural adhesive joints using double cantilever beam and tapered double cantilever beam specimens, 61010-1 © Iec:2001.
Kendall, K., 1975. Control of cracks by interfaces in composites. Proc. R. Soc. London. A. Math. Phys. Sci. 341, 409–428. https://doi.org/10.1098/rspa.1975.0001
Kermani, N.N., Simacek, P., Advani, S.G., 2020. Porosity predictions during co-cure of honeycomb core prepreg sandwich structures. Compos. Part A Appl. Sci. Manuf. 132, 105824. https://doi.org/10.1016/j.compositesa.2020.105824
Khan, R., 2019. Fiber bridging in composite laminates: A literature review. Compos. Struct. 229. https://doi.org/10.1016/j.compstruct.2019.111418
Kim, G.H., Choi, J.H., Kweon, J.H., 2010. Manufacture and performance evaluation of the composite hat-stiffened panel. Compos. Struct. 92, 2276–2284. https://doi.org/10.1016/j.compstruct.2009.07.019
Kinloch, A.J., Shaw, S.J., 1981. The Fracture Resistance of a Toughened Epoxy Adhesive. J. Adhes. 12, 59–77. https://doi.org/https://doi.org/10.1080/00218468108071189
Kuwata, M., Hogg, P.J., 2011. Interlaminar toughness of interleaved CFRP using non-woven veils: Part 1. Mode-I testing. Compos. Part A Appl. Sci. Manuf. 42, 1551–1559. https://doi.org/10.1016/j.compositesa.2011.07.016
Li, X., Lu, S., Lubineau, G., 2021. Snap-back instability of double cantilever beam with bridging. Int. J. Solids Struct. 233, 111150. https://doi.org/10.1016/j.ijsolstr.2021.111150
Maloney, K., Fleck, N., 2019. Toughening strategies in adhesive joints. Int. J. Solids Struct. 158, 66–75. https://doi.org/10.1016/j.ijsolstr.2018.08.028
Maloney, K., Fleck, N., 2018. Damage tolerance of an architected adhesive joint. Int. J. Solids Struct. 132–133, 9–19. https://doi.org/10.1016/j.ijsolstr.2017.06.010
Martiny, P., Lani, F., Kinloch, A.J., Pardoen, T., 2012. A multiscale parametric study of mode i fracture in metal-to-metal low-toughness adhesive joints. Int. J. Fract. 173, 105–133. https://doi.org/10.1007/s10704-011-9667-x
Min, H.S., Kim, S.C., 1999. Fracture toughness of polysulfone/epoxy semi-IPN with morphology spectrum. Polym. Bull. 42, 221–227. https://doi.org/10.1007/s002890050456
Morano, C., Zavattieri, P., Alfano, M., 2020. Tuning energy dissipation in damage tolerant bio-inspired interfaces. J. Mech. Phys. Solids 141, 103965. https://doi.org/10.1016/j.jmps.2020.103965
Pardoen, T., Ferracin, T., Landis, C.M., Delannay, F., 2005. Constraint effects in adhesive joint fracture. J. Mech. Phys. Solids 53, 1951–1983. https://doi.org/10.1016/j.jmps.2005.04.009
Pocius, A. V., 2012. Adhesion and Adhesives Technology, Third Edit. ed, Adhesion and Adhesives Technology. Carl Hanser Verlag GmbH & Co. KG. https://doi.org/10.3139/9783446431775.fm
Quan, D., Bologna, F., Scarselli, G., Ivankovic, A., Murphy, N., 2020. Interlaminar fracture

toughness of aerospace-grade carbon fibre reinforced plastics interleaved with thermoplastic veils. Compos. Part A Appl. Sci. Manuf. 128, 105642. https://doi.org/10.1016/j.compositesa.2019.105642

Quan, D., Farooq, U., Zhao, G., Dransfeld, C., Alderliesten, R., 2022. Co-cured carbon fibre/epoxy composite joints by advanced thermoplastic films with excellent structural integrity and thermal resistance. Int. J. Adhes. Adhes. 118, 103247. https://doi.org/10.1016/j.ijadhadh.2022.103247

Quan, D., Ma, Y., Yue, D., Liu, J., Xing, J., Zhang, M., Alderliesten, R., Zhao, G., 2023. On the application of strong thermoplastic–thermoset interactions for developing advanced aerospace-composite joints. Thin-Walled Struct. 186, 110671. https://doi.org/10.1016/j.tws.2023.110671

Reedy, J.D., 2008. Effects of patterned nanoscale interfacial roughness on interfacial toughness: A finite element analysis. J. Mater. Res. 23, 3056–3065. https://doi.org/10.1557/JMR.2008.0369

Sørensen, B.F., Jacobsen, T.K., 1998. Large-scale bridging in composites: R-curves and bridging laws. Compos. Part A Appl. Sci. Manuf. 29, 1443–1451. https://doi.org/10.1016/S1359-835X(98)00025-6

Spearing, S.M., Evans, A.G., 1992. The role of fiber bridging in the delamination resistance of fiber-reinforced composites. Acta Metall. Mater. 40, 2191–2199. https://doi.org/10.1016/0956-7151(92)90137-4

Szekrényes, A., Uj, J., 2005. Advanced beam model for fiber-bridging in unidirectional composite double-cantilever beam specimens. Eng. Fract. Mech. 72, 2686–2702. https://doi.org/10.1016/j.engfracmech.2005.05.001

Tao, R., Li, X., Yudhanto, A., Alfano, M., Lubineau, G., 2022. Toughening adhesive joints through crack path engineering using integrated polyamide wires. Compos. Part A Appl. Sci. Manuf. 158, 106954. https://doi.org/10.1016/j.compositesa.2022.106954

van Innis, C., Pardoen, T., 2023. Thickness-dependent selection of adhesive joints. J. Adhes. 00, 1–54. https://doi.org/10.1080/00218464.2023.2294131

Van Loock, F., Thouless, M.D., Fleck, N.A., 2019. Tensile fracture of an adhesive joint: the role of crack length and of material mismatch. J. Mech. Phys. Solids 130, 330–348. https://doi.org/10.1016/j.jmps.2019.06.004

Van Velthem, P., Ballout, W., Daoust, D., Sclavons, M., Cordenier, F., Henry, E., Dumont, D., Destoop, V., Pardoen, T., Bailly, C., 2015. Influence of thermoplastic diffusion on morphology gradient and on delamination toughness of RTM-manufactured composites. Compos. Part A Appl. Sci. Manuf. 72, 175–183. https://doi.org/10.1016/j.compositesa.2015.02.012

Voleppe, Q., Ballout, W., Velthem, P. Van, Bailly, C., Pardoen, T., 2021. Enhanced fracture resistance of thermoset / thermoplastic interfaces through crack trapping in a morphology gradient. Polymer (Guildf). 218, 123497. https://doi.org/10.1016/j.polymer.2021.123497

Xia, S.M., Ponson, L., Ravichandran, G., Bhattacharya, K., 2013. Adhesion of heterogeneous thin films - I: Elastic heterogeneity. J. Mech. Phys. Solids 61, 838–851. https://doi.org/10.1016/j.jmps.2012.10.014

Yudhanto, A., Almulhim, M., Kamal, F., Tao, R., Fatta, L., Alfano, M., Lubineau, G., 2020. Enhancement of fracture toughness in secondary bonded CFRP using hybrid thermoplastic/thermoset bondline architecture. Compos. Sci. Technol. 199, 108346. https://doi.org/10.1016/j.compscitech.2020.108346

Zavattieri, P.D., Hector, L.G., Bower, A.F., 2007. Determination of the effective mode-I toughness of a sinusoidal interface between two elastic solids. Int. J. Fract. 145, 167–180. https://doi.org/10.1007/s10704-007-9109-y